



Repositorio Institucional de la Universidad Autónoma de Madrid

<https://repositorio.uam.es>

Esta es la **versión de autor** del artículo publicado en:

This is an **author produced version** of a paper published in:

SENSORS AND ACTUATORS B: CHEMICAL, 10 April (2018)

DOI: <http://doi.org/10.1016/j.snb.2018.03.179>

Copyright: © 2018 Elsevier Ltd.

El acceso a la versión del editor puede requerir la suscripción del recurso

Access to the published version may require subscription

Gold nanoparticle triggered dual optoplasmonic-impedimetric sensing of prostate-specific antigen on interdigitated porous silicon platforms

C. Rodríguez^{1,2}, V. Torres Costa^{1,3}, O. Ahumada², V. Cebrián², C. Gómez-Abad², A. Díaz², M Manso Silván^{1*}

¹Departamento de Física Aplicada and Instituto de Ciencia de Materiales Nicolás Cabrera, Universidad Autónoma de Madrid, 28049, Madrid, Spain

²Mecwins S.L., Parque Científico de Madrid PTM, C/Santiago Grisolia 2, Tres Cantos, 28760, Madrid, Spain

³Centro de Microanálisis de Materiales, Universidad Autónoma de Madrid, 28049, Madrid, Spain

*corresponding author: chloe.rodriguez@uam.es, tel: +34 914974919

Abstract

A porous silicon (PSi) platform with interdigitated NiCr electrodes has been used for the impedimetric biosensing of prostate specific antigen (PSA), a cancer biomarker. The first step involved the formation of a conductive PSi structure through the ion beam creation of 200 nm deep interdigitated slots, followed by their filling with NiCr electrodes deposited by plasma sputtering. In the second step a biorecognition interface was formed by modification of the PSi surface with (3-Glycidyloxypropyl)-trimethoxysilane. A sandwich assay was performed in which PSA was first recognized by a surface-anchored antibody and then by a secondary antibody tethered to 100 nm gold nanoparticles (GNPs). The changes in the impedance upon analyte binding at different concentrations have been monitored showing that the PSA concentration exhibits a linear dependence with the series resistance defined from the device equivalent circuit. A limit of detection in the range of 1 ng/mL PSA has been determined. A dark-field study of the PSi surface after the sandwich bioassay allowed an optoplasmonic demonstration of the increasing density of GNPs at higher PSA concentrations, which was confirmed by using scanning electron microscopy. The results confirm the dual optoplasmonic-electric labelling effect of the 100 nm GNPs and their role in an internally controlled detection of PSA.

Keywords: porous silicon, impedance, biosensor, sandwich bioassay, gold nanoparticles.

1 Introduction

Prostate cancer is the most common form of cancer in males and the second leading cause of cancer related death. MicroRNAs [1] and prostate specific antigen (PSA) are the two main challenging prostate cancer biomarkers. In particular, PSA is a protein biomarker produced by the cells of prostate gland and whose normal level in blood is elevated when affected by prostate cancer [2,3]. Nowadays, there are only two approved prostate cancer screening methods. In view of the ineffective diagnostic by digital rectal examination, clinicians are increasingly turning to less invasive blood-based diagnostic tests, which have led to important improvements in early detection. Several techniques such as micro-fluidic chips [4], nanoparticle sensors [5], piezoelectric crystals [6,7], etc, are therefore applied. In particular, electrochemical impedance spectroscopy- (EIS-) based detection is playing a significant role as a label-free technique for sensitive measurement of PSA [8-10] thanks to its high sensitivity and selectivity, miniaturization potential, simplicity and affordability [11-13].

A typical EIS biosensor comprises a sensing element consisting of a conducting surface onto which capture molecules are immobilized to induce the specific binding and recognition and to target the protein of interest. Finally, the electrical impedance at the interface is measured in steady-state conditions. In particular, impedance biosensors using interdigitated electrodes have been extensively employed for label free and rapid detection of a wide variety of biomolecules [14-16]. However, they suffer from limited sensitivity and risk of loss of specificity. To improve the performances, porous silicon (PSi) is a good candidate to replace the conventional substrates in novel chemical sensors and biosensors [17]. The high specific surface area of PSi together with the control of the physico-chemical behavior of its nanostructured surface, make of this material a versatile substrate for the development of sensors. Moreover, its

biocompatibility and biodegradability open the way to the development of implantable biosensors. In particular, the electrical behavior of PSi is in general extremely sensitive to its surface properties and composition, and is highly sensitive to the presence or absence of biomolecules on its surface [18].

The sensitivity of the biosensors can be increased using different types of nanoparticles, such as metallic nanoparticles [19-21], quantum dots [22] or magnetic nanoparticles [19]. Indeed, owing to their unique properties, gold nanoparticles (GNPs) are often used as carriers for signal amplification in biosensors. In particular, due to their biocompatibility, their optical and electronic properties, and their remarkable versatility in bio medical applications, they are mostly used as signal transducers for biosensor applications [10,20]. The majority of GNP-based assays exploit their surface plasmon absorption [23,24], their ability to quench fluorescence [25] or simply their contribution to adsorbed mass [26]. This versatility allows proposing a series of sensors with increased sensitivity or internal controls.

In the present work, we propose the use of a PSi substrate with NiCr interdigitated electrodes as a conductive platform in order to fabricate an impedance biosensor for the detection of PSA. We consider a sandwich bioassay with 100 nm GNPs to enhance the conductivity of the surface, while at the same time remaining an optoplasmonic label. In fact, in this size range the GNPs are small enough to induce plasmons, but are big enough to allow a microscopic detection of the scattering (no contribution to background) [26].

2. Experimental

The whole process of preparation of the NiCr/PSi impedimetric interface and the protocols for its use as a GNP enhanced biosensor are illustrated in figure 1.

2.1 Preparation of PSi samples

The back side of p-type boron-doped (resistivity 0.05–0.1 $\Omega\cdot\text{cm}$) (100) oriented Si wafers were first coated with an aluminum layer to provide low resistance ohmic electrical contacts, and subsequently cut into 15 mm \times 15 mm pieces, which were mounted into a Teflon electrochemical cell anode. Spongy-type PSi was then fabricated by electrochemical etching of the silicon wafer in an aqueous electrolyte composed of a mixture of hydrofluoric acid (HF) and absolute ethanol (volume ratio 1:1). The current density was fixed at 80mA/cm², and the anodization time at 20s. The samples were then rinsed with ethanol and dried with N₂. After anodization, samples were submitted to chemical oxidation in solution of H₂O₂/EtOH (volume ratio 1:1) for 30 min, as a way of stabilizing the surface and reducing possible reactions with the ambient.

2.2 Formation of electrical contacts

In order to allow the impedance measurements, interdigitated Ni/Cr electrical contacts were created on the front PSi. The first step involved the formation of slots by ion etching following a specific pattern by means of a Si mask (Figure 1). For that, we performed a 0.5 KeV Ar ion bombardment by means of a Kaufman ion source operated at 10⁻³ mbar. A total charge of 0.6 C was applied to obtain slots of about 250 nm deep. A Ni/Cr (40/60 wt %) alloy was then sputtered by Ar⁺ ions in a low-pressure supported discharge in the previously created slots. Once the PSi sample was introduced in the vacuum chamber, argon was introduced to the chamber until a sputtering pressure of 1 x 10⁻² mbar was reached. A current of 1 A and a voltage of 0.5 kV were then applied to strike a sputtering plasma and the shutter opened once a pre-sputter sequence of 5 min

was finished. The deposition time was 5 min. Once the process was finished, the Si mask was removed giving rise to the resulting NiCr/PSi structure.

2.3 Formation of a biorecognition interface

We performed a sandwich assay for the detection of PSA (Fig.2) [26]. This experiment involves two biorecognition steps to enhance the selectivity and to amplify the sensor response. This first step includes a silanization at room temperature with (3-Glycidyloxypropyl)trimethoxysilane (GPTMS) (Sigma-Aldrich), a molecule containing an epoxy group, which reacts with the SiOH groups on the surface of PSi (formed by the chemical oxidation) leading to a large surface density of epoxy groups [27,28]. Then, the capture antibody (monoclonal mouse anti-prostate specific antigen 1H12 antibody) is immobilized on the PSi surface for 2 h at 37°C at a concentration of 50 µg/mL in 10 mM MES (pH 3.8), and the free surface is blocked with (aminoethyl)polyethylene glycol (PEG) (Sigma-Aldrich) at 1 mg/mL in 10 mM MES with 0.05% Tween[®] (pH 5.5) overnight and 4°C in order to avoid non-specific interactions. Then, an immunoreaction between PSA and the capture antibodies takes place by immersion of PSi-based devices in PSA:fetal bovine serum (FBS) 1x in a range of concentrations from 0.1 to 500 ng/mL at 37°C. The control is performed in FBS without PSA. Finally, a sandwich assay takes place by immersion at 37°C for 1h of the PSi samples in a 5 µg/mL solution prepared in MES (pH 3.8) with 0.05% Tween[®] of spherical 100 nm diameter GNPs coated with 2-3 nm long thiol-spacer-carboxyl (C11-100-TC-50, NanopartzTM) and functionalized with the secondary antibody (anti-prostate specific antigen 5A6 antibody). The secondary antibody was immobilized onto the surface of the carboxyl-polymer coated GNPs following the procedure provided by NanopartzTM (<http://www.nanopartz.com/>) [26]. Monoclonal mouse antibodies against

prostate specific antigen (1H12 and 5A6) and PSA from human seminal fluid were purchased from HyTest (Turku, Finland).

2.4 Impedance measurements

Impedance measurements were performed with a SP-150 instruments (Bio-Logic Science Instruments) and measured between two points of the NiCr pattern. A voltage amplitude of 500 mV and a frequency range of 500 mHz-200 kHz at a base potential of 0 mV was applied. All measurements were carried out at room temperature after phase and amplitude calibration with a known R and an RC pattern circuit.

3. Results

3.1 Device characterization.

The images shown in Figure 2 highlight the structure of the different parts of the NiCr/PSi impedimetric device. Since PSi is in general a poor electrical transducer of very low conductivity, we formed interdigitated NiCr electrical contacts on its surface. The general surface view of the device is shown in figure 2.a, where the interferometry colored PSi layer appears partially covered by the metallic interdigitated NiCr electrode. The good interfacial adherence at the NiCr/PSi and PSi/Si interfaces is outlined in the SEM image of figure 2.b. The NiCr layer has a thickness of 270 nm and does not penetrate the pores. Columns of NiCr grow on a well-defined surface induced by the ion bombardment, giving rise to standard column width of 40 nm. We obtained a sponge-like PSi layer with interconnected pores (Fig. 2.c) that can be clearly seen in the higher magnification SEM image (inset). The homogeneity of the NiCr contact on the PSi surface is outlined in the SEM image of Fig. 2.d. The internal structure of PSi and NiCr surfaces are magnified in the corresponding SEM images. On the one hand, one can

observe the crater like structure of the PSi surface (Figure 2.e) with mean surface pore radius of 30 nm. On the other hand, the surface of the NiCr contact is granular with grain size in good agreement with the columnar width observed in the cross section images (Fig. 2.f).

We measured the impedance at the interface of the PSi-based device. For that, we applied an alternating signal of 500 mV of amplitude to the NiCr pattern, performed a frequency sweep in the range of 500 mHz-200 kHz and obtained the corresponding Nyquist diagram (Figure 3). An equivalent circuit based on a combination of two resistors (R_1 and R_2) and a constant phase element (CPE) (Q_2) (Figure 3 inset) was used to fit the experimental data with the theoretical model. The CPE is an equivalent circuit component that models the behaviour of a double/multiple layer behaving as an imperfect capacitor. Physically, it represents a heterogeneous capacitance very often due to the surface roughness of the sample, which can be physically explained in our system in view of the porosity of PSi, and even the granular nature of the NiCr device. Indeed, the difference between a capacitor C and a CPE Q is that the expression of the impedance of a CPE contains an additional parameter α :

$$Z_Q(f) = \frac{1}{Q(j2\pi f)^\alpha} \quad \text{Eq. 1}$$

where α is comprised between 0 and 1, and $Z_Q(f) = Z_C(f)$ for $\alpha = 1$, that is, an ideally planar capacitor. R_2 is a resistance associated to the transfer efficiency at the PSi/NiCr junction and is thus considered in parallel to the constant phase element. Finally, R_1 represents the transport of charge through the functionalized PSi surface. With this selection, the final equivalent circuit for the NiCr/PSi device was observed to behave as:

$$Z(f) = R_1 + \frac{R_2}{R_2 Q_2 (j2\pi f)^{\alpha_2} + 1} \quad \text{Eq. 2}$$

3.2 Sandwich bioassay for the detection of PSA

Changes in the interfacial impedance upon binding of PSA-GNPs conjugates in the concentration range 0.1 ng/mL–500 ng/mL in PBS were then measured. Figure 4.a shows the Nyquist representation obtained for binding experiments performed with different concentrations of PSA. The curves can be fitted with the theoretical model used in Eq. 2. The values associated to the model parameters were extracted from the fitting and are resumed in Table 1. We can observe that the values of the R_1 resistors decrease with the concentration of PSA, while those of the CPE increase. The value of the surface impedance at a frequency of 500 mHz (maximum impedance) for each concentration shows a nonlinear decay with increasing diminution rate of the impedance for increasing concentrations. Meanwhile, the dependence of R_1 with respect to the concentration of PSA in the range 0.1-500 ng/mL shows a linear decay dependence (Fig. 4.b). A linear fit to the plot allows obtaining the following calibration line for R_1 by using the NiCr/PSi impedimetric device:

$$R_1 (\Omega) = 9539 - 12.05 [\text{PSA}] (\text{ng/mL})$$

The analytical limit of this calibration line can be established at 1 ng/mL PSA, in view of the partial error bar overlap of the 0.1 ng/mL point with the zero concentration control. To analyze the mechanism of transduction in more detail, it is worth underlining that the decrease in the value of the equivalent resistors with PSA concentration implies that the surface is becoming more conductive. This can be intuitively attributed to the increased surface density of GNPs bound to the PSA

molecules. Relevantly, the presence of the thiolated spacer and conjugated antibody do not significantly alter the contribution of GNPs to the conductivity since they do not induce a compact shell structure.

To confirm the relationship between conductivity and density of GNPs, we analyzed the surfaces of the impedimetric devices after performing the sandwich assay by dark-field and electron microscopy. Gold nanoparticles gave rise to clear light scattering contrast on the surface of the PSi surface (Fig. 5, top inset). To unequivocally identify the GNPs and differentiate from scattering on Si due to the PSi nanotopography, the surface was further analyzed by SEM (Fig. 5, bottom inset). The correlated counting of the GNPs on the PSi surface for the different concentrations of PSA gave rise to the central graph of Figure 5. The density of GNPs shows a linear dependence on the PSA concentration in the range used in this experiment. This result suggests in fact that there is an indirect relationship between the density of GNPs on the surface and the equivalent resistance R_1 of the NiCr/PSi device upon binding with different concentrations of PSA. Additionally, this inverse relationship is clue in the habilitation of an internal control of the device making use of the dual optoplasmonic-electric transduction of the 100 nm GNPs. These results invite to pursue further research on the use of GNP supported PSi impedimetric biosensors.

4. Conclusions

An impedimetric device based on PSi with a NiCr interdigitated electrode was fabricated and characterized. PSA was immobilized at different concentrations on its surface and the sensitivity analyzed in a sandwich bioassay enhanced by 100 nm GNPs. The increasing immobilization of the protein biomarker resulted in a decreasing impedance within the 0.1 to 500 ng/mL. The series resistance obtained from the

equivalent circuit showed a linear dependence with the concentration of PSA and allowed obtaining a calibration line for the biosensor and determining a limit of detection at 1 ng/mL. PSi has a high initial impedance, which allows obtaining large impedance contrasts after the analyte binding and further exposure to the GNPs. Indeed, the GNPs allow increasing the sensitivity of the detection due to their contribution to the device conductivity. A dark field microscopic analysis outlined the possibility of performing a dual detection since the immobilization of 100 nm GNPs introduces visible hot-spots. Consequently, the concentration of PSA bound on the PSi surface could be correlated with the density of immobilized GNPs. Accordingly, this PSi-GNP based platform could be a possible candidate for the development of dual electric-optoplasmonic biosensors for PSA detection, with the added value of presence of an internal transduction control.

Acknowledgments

Authors thank L. García Pelayo for his technical assistance during materials processing. We acknowledge MSC funding provided by the European Commission through FPVII grant THINFACE (ITN GA 607232).

Reference List

- [1] K. Hudcova, L. Trnkova, I. Kejnovska, M. Vorlickova, J. Gumulec, R. Kzek, M. Masarik, Novel biophysical determination of miRNAs related to prostate and head and neck cancers, *European Biophysics Journal*. 44 (2015) 131-138.
- [2] M.A. Najeeb, S. Jasmine, M. Chavali, Recent advancements in nano-based biosensor for early detection of prostate cancer, *International Journal of recent trends in electrical & electronics engineering*. 3 (2014) 112-120.

- [3] M.A. Najeeb, S. Pillai, M. Chavali, Nano-based PSA biosensors: an early detection technique of prostate cancer, *Journal of Biomimetics, Biomaterials and Biomedical Engineering*. 20 (2014) 87-98.
- [4] N. Triroj, P. Jaroenapibal, H. Shi, J.I. Yeh, R. Beresford, Microfluidic chip-based nanoelectrode array as miniaturized biochemical sensing platform for prostate-specific antigen detection, *Biosensors and Bioelectronics*. 26 (2011) 2927-2933.
- [5] D.A. Healy, C.J. Hayes, P. Leonard, L. McKenna, R. O'Kennedy, Biosensor developments: application to prostate-specific antigen detection, *Trends in Biotechnology*. 25 (2007) 125-131.
- [6] Y. Ding, H. Lu, G. Shi, J. Liu, G. Shen, R. Yu, Cell-based immobilization strategy for sensitive piezoelectric immunoassay of total prostate specific antigen, *Biosensors and Bioelectronics*. 24 (2008) 228-232.
- [7] R. Gupta, S. Swaminathan, Modeling and simulation of piezoelectric based micro cantilever systems for prostate specific antigen, *International Symposium on Next-Generation Electronics (ISNE)*. (2015).
- [8] G. Chornokur, S.K. Arya, C. Phelan, R. Tanner, S. Bhansali, Impedance-based miniaturized biosensor for ultrasensitive and fast prostate-specific antigen detection, *Journal of Sensors*. 2011 (2011) 1-7.
- [9] S.K. Arya, S. Bhansali, Anti-prostate specific antigen (anti-PSA) modified interdigitated microelectrode-based impedimetric biosensor for PSA detection, *Biosensors Journal*. 1 (2012) 1-7.
- [10] L.T.N. Truong, T.T. Nguyen, A.L.T. Luu, Y. Ukita, Y. Takamura, Sensitive labels impedance immunosensor using gold nanoparticles-modified of screen-printed carbon ink electrode for ACT-prostate specific antigen detection, *16th International Conference on Miniaturized Systems for Chemistry and Life Sciences*. (2012) 1912-1914.
- [11] R. Radhakrishnan, I.I. Suni, C.S. Bever, B.D. Hammock, Impedance biosensors: applications to sustainability and remaining technical challenges, *ACS Sustainable Chemistry & Engineering*. 2 (2014) 1649-1655.
- [12] J.S. Daniels, N. Pourmand, Label-free impedance biosensors: opportunities and challenges, *Electroanalysis*. 19 (2007) 1239-1257.
- [13] K. Kant, C. Priest, J.G. Shapter, D. Losic, The influence of nanopore dimensions on the electrochemical properties of nanopore arrays studied by impedance spectroscopy, *Sensors*. 14 (2014) 21316-21328.
- [14] R. Ohno, H. Ohnuki, H. Wang, T. Yokoyama, H. Endo, D. Tsuya, M. Izumi, Electrochemical impedance spectroscopy biosensor with interdigitated electrode for detection of human immunoglobulin A, *Biosensors and Bioelectronics*. 40 (2013) 422-426.

- [15] L. Yang, Y. Li, C.L. Griffis, M.G. Johnson, Interdigitated microelectrode (IME) impedance sensor for the detection of viable *salmonella typhimurium*, Biosensors and Bioelectronics. 19 (2004) 1139-1147.
- [16] R. Wang, J. Lum, Z. Callaway, J. Lin, W. Bottje, Y. Li, A label-free impedance immunosensor using scree-printed interdigitated electrodes and magnetic nanobeads for the detection of *E. Coli* O157:H7, Biosensors. 5 (2015) 791-803.
- [17] N. Naveas, J. Hernandez-Montelongo, R. Pulido, V. Torres-Costa, R. Villanueva-Guerrero, J.P. García Ruiz, M. Manso-Silván, Fabrication and characterization of a chemically oxidized-nanostructured porous silicon based biosensor implementing orienting protein A, Colloids and Surfaces B: Biointerfaces. 115 (2014) 310-316.
- [18] G. Recio-Sánchez, V. Torres-Costa, M. Manso, D. Gallach, J. López-Garcia, R.J. Martín-Palma, Toward the development of electrical biosensors based on nanostructured porous silicon, Materials. 3 (2010) 755-763.
- [19] J. Lei, H. Ju, Signal amplification using nanomaterials for biosensing, Chemical sensors and biosensors. 14 (2013) 17-42.
- [20] H. Hutter, D. Maysinger, Gold-nanoparticle-based biosensors for detection of enzyme activity, Trends in Pharmacological Sciences. 34 (2013) 497-507.
- [21] M. Mathelié-Guinlet, I. Gammoudi, L. Beven, F. Moroté, M. Delville, C. Grauby-Heywang, T. Cohen-Bouhacina, Silica nanoparticles assisted electrochemical biosensor for the detection and degradation of *Escherichia Coli* bacteria, Procedia Engineering. 168 (2016) 1048-1051.
- [22] M. Holzinger, A. Le Goff, S. Cosnier, Nanomaterials for biosensing applications: a review, Frontiers in Chemistry. 2 (2014) 1-10.
- [23] R.A. Reynolds, C.A. Mirkin, R.L. Letsinger, Homogeneous nanoparticle-based quantitative colorimetric detection of oligonucleotides, Journal of American Chemical Society. 122 (2000) 3795-3796.
- [24] W. Xu, X. Xue, T. Li, H. Zeng, X. Liu, Ultrasensitive and selective colorimetric DNA detection by nicking endonuclease assisted nanoparticle amplification, Angewandte Chemie International Edition. 48 (2009) 6849-6852.
- [25] J. Zhu, J. Li, A. Wang, Y. Chen, J. Zhao, Fluorescence quenching of alpha-fetoprotein by gold nanoparticles: effect of dielectric shell on non-radioactive decay, Nanoscale Research Letters. 5 (2010) 1496-1501.
- [26] P.M. Kosaka, V. Pini, J.J. Ruz, R.A. da Silva, M.U. González, D. Ramos, M. Calleja, J. Tamayo, Detection of cancer biomarkers in serum using a hybrid mechanical and optoplasmonic nanosensor, Nature Nanotechnology. 9 (2014) 1047.
- [27] F. Frascella, S. Ricciardi, L. Pasquardini, C. Potrich, A. Angelini, A. Chiadò, C. Pederzoli, N. De Leo, P. Rivolo, C.F. Pirri, E. Descrovi, Enhanced fluorescence detection of miRNA-16 on a photonic crystal, Analyst. 140 (2015).

[28] C. Rodriguez, O. Ahumada, V. Cebrián, V. Torres Costa, M. Manso Silván, Biofunctional porous silicon micropatterns engineered through visible light activated epoxy capping and selective plasma etching, *Vacuum*. 150 (2018) 232-232.

Figures and Tables

Table 1. Parameters obtained after fitting of the experimental bioassay frequency sweep curves to the equivalent circuit of equation 2 and maximum value of the impedance (Z (500 mHz)).

	[PSA] (ng/mL)						
	0	0.1	1	10	100	250	500
$R_1 (\Omega)$	9550 ± 7	9545 ± 7	9530 ± 6	9400 ± 8	8484 ± 9	6364 ± 7	3562 ± 6
$\frac{Q_2}{(F_s^{(a_2-1)})} / \times 10^{-7}$	1.31 ± 0.02	1.34 ± 0.02	1.38 ± 0.05	1.59 ± 0.04	2.78 ± 0.02	7.99 ± 0.05	9.82 ± 0.07
a_2	0.76 ± 0.01	0.77 ± 0.03	0.76 ± 0.01	0.82 ± 0.01	0.75 ± 0.03	0.67 ± 0.03	0.60 ± 0.01
$R_2 (\Omega) / \times 10^7$	3.4 ± 0.1	2.1 ± 0.1	1.6 ± 0.2	0.9 ± 0.2	0.64 ± 0.04	0.58 ± 0.02	0.18 ± 0.05
$Z_{MAX} (k\Omega)$	9000 ± 300	8200 ± 500	7300 ± 200	5400 ± 500	3400 ± 200	1500 ± 300	800 ± 200

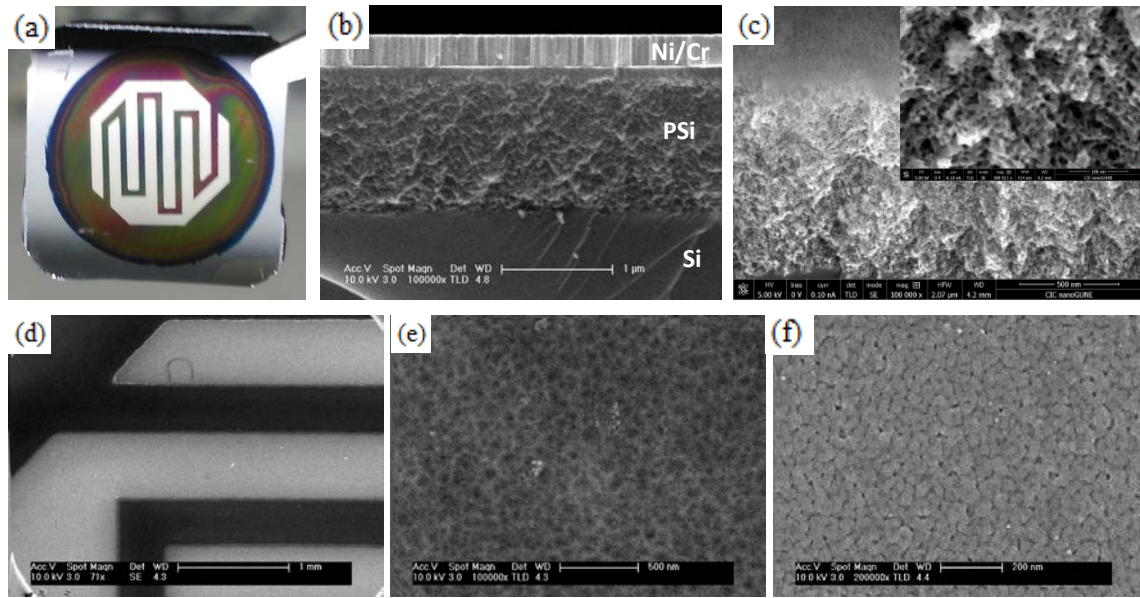


Figure 2. (a) General image of the NiCr/PSi impedimetric structure (PSi area has 1 cm radius). (b) SEM cross-section image of the NiCr/PSi/Si stack, (c) Magnified SEM image of the PSi interface with inset to illustrate the spongy form PSi. (d) Surface view SEM image of the NiCr electrode on the PSi surface and corresponding SEM magnifications of the surface morphology (e) on the PSi layer, and (f) on the Ni/Cr layer.

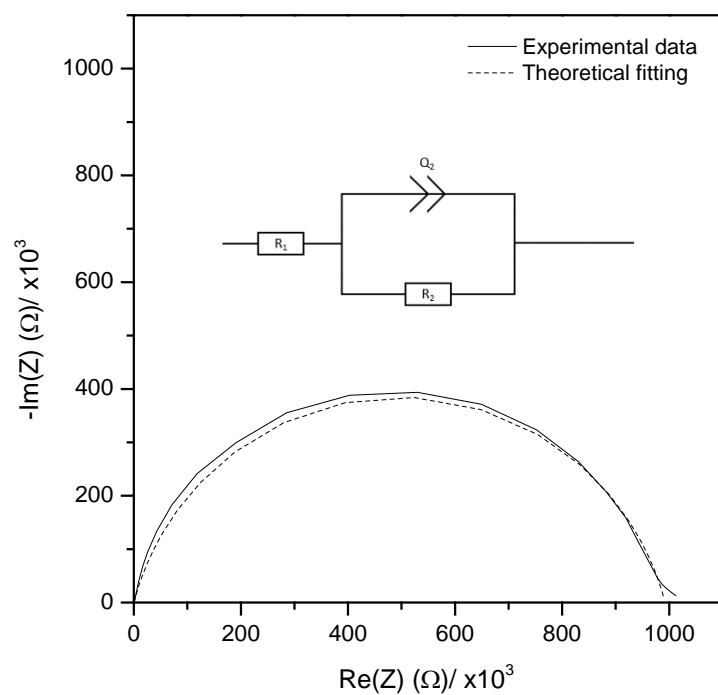


Figure 3. Nyquist representation of the frequency sweep (500 mHz-200 kHz) analysis performed onto the NiCr/PSi device and its corresponding equivalent circuit (inset).

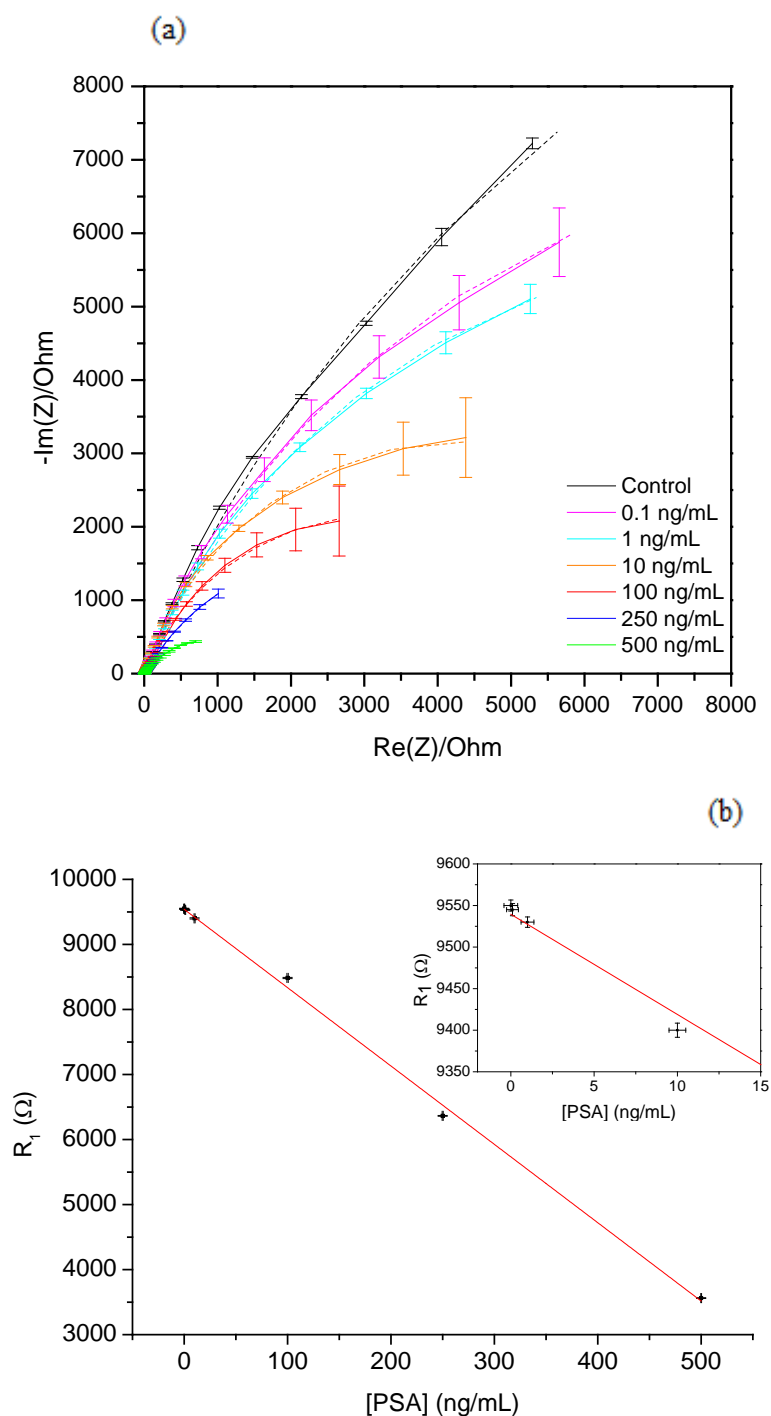


Figure 4. (a) Nyquist representation of the frequency sweep analysis performed on the NiCr/PSi device after binding at concentrations of PSA and sandwiching with 100 nm GNPs. — Experimental data and - - - - - theoretical fitting. (b) Concentration of PSA as a function of the equivalent series resistance R_1 . Inset: linear fitting magnification at the high R_1 range.

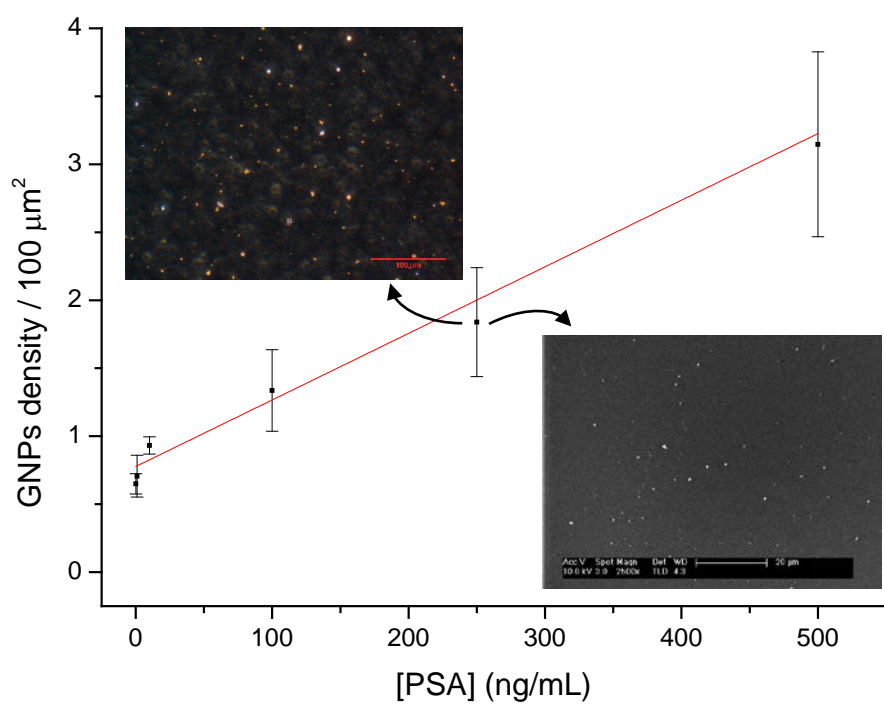


Figure 5. GNPs density on the PSi surface as a function of the PSA concentration in FBS as extracted from correlated estimations by dark-field and scanning electron microscopy. Inset images for illustration correspond to PSA concentrations of 250 ng/mL. Identification of the optoplasmonic hotspots in 100 nm GNPs (Dark field, top) and secondary electrons contrast (SEM, bottom).